Supplementary Information for

Boosted ammonium production by single cobalt atom catalysts with high Faradic efficiencies

Jiacheng Li, Miao Li*, Ning An, Shuo Zhang, Qinan Song, Yilin Yang, Jing Li, Xiang Liu

School of Environment, Tsinghua University, 30# Shuangqing Road, Hai Dian District, Beijing, 100086, China.

*E-mail: miaoli@tsinghua.edu.cn; Tel.: 86-10-62772485.

This PDF file includes:

Figures S1 to S15
Table S1 to S3
References for SI reference citations

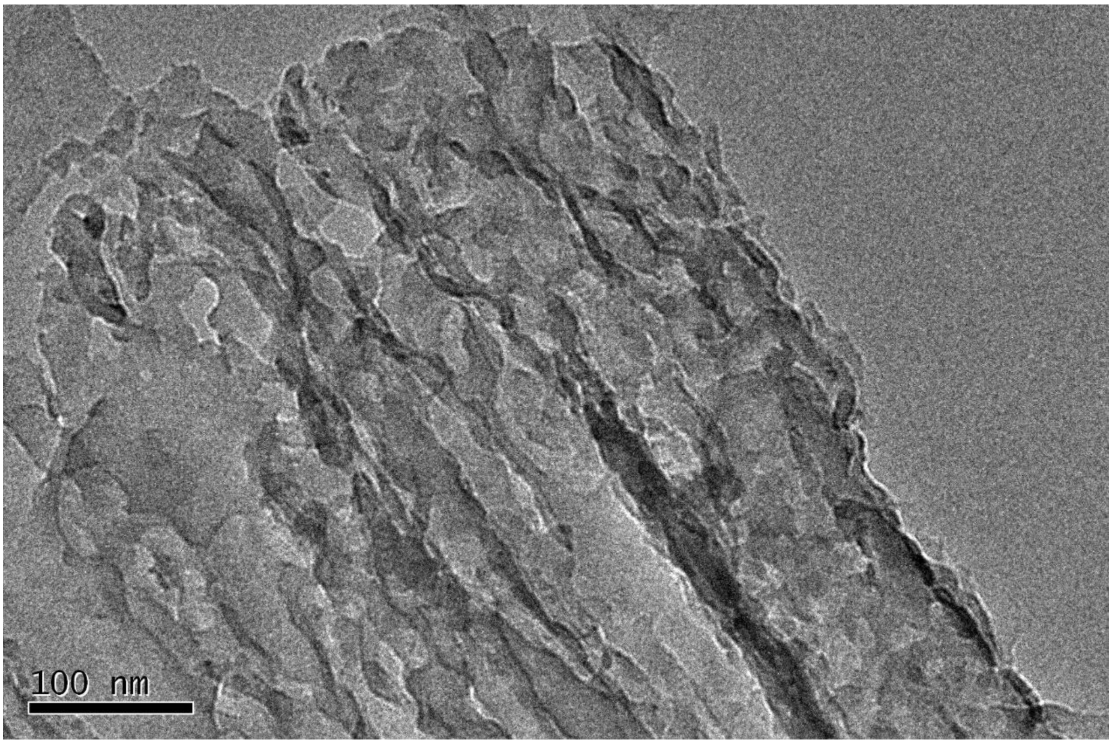

Supplementary Figure 1. TEM images of Co-CN.

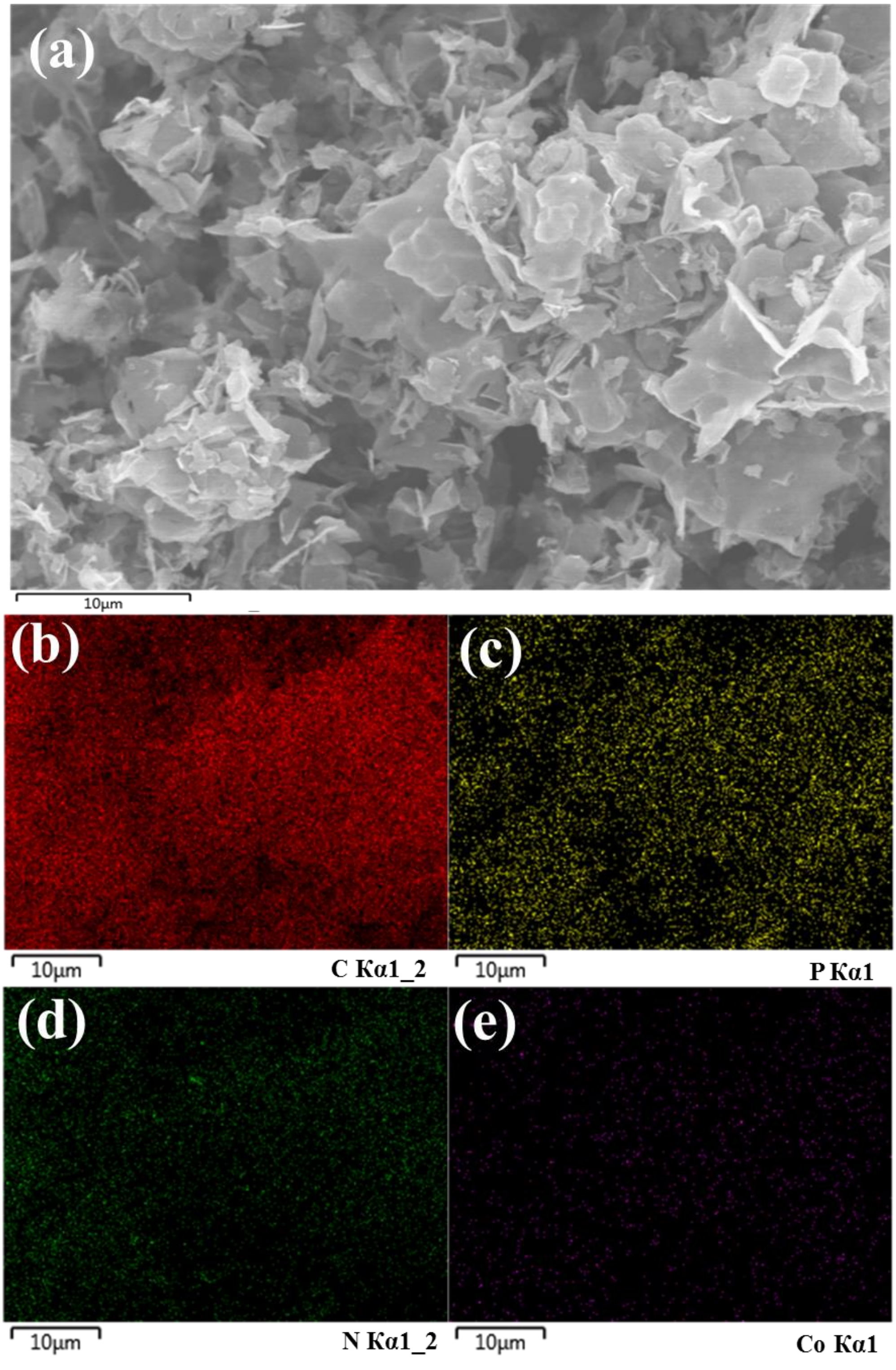

Supplementary Figure 2. SEM image of Co-CNP and its energy-dispersive spectroscopy (EDS): C (red), P (blue), N (green), and Co (purple)

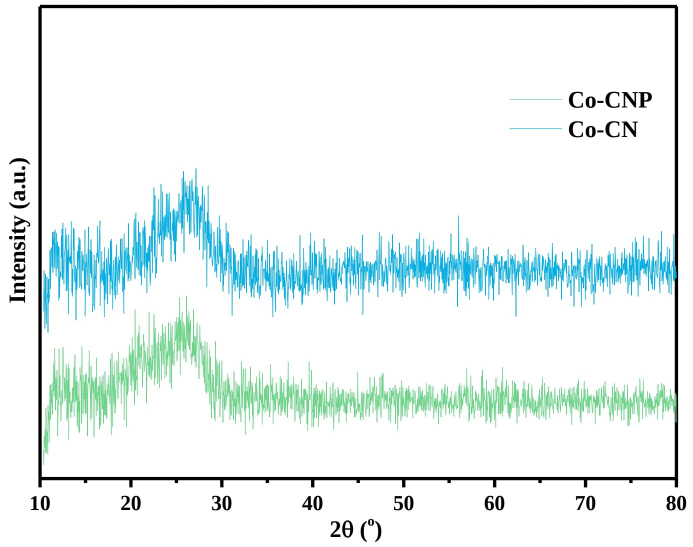

Supplementary Figure 3. XRD patterns of Co-CN and Co-CNP.

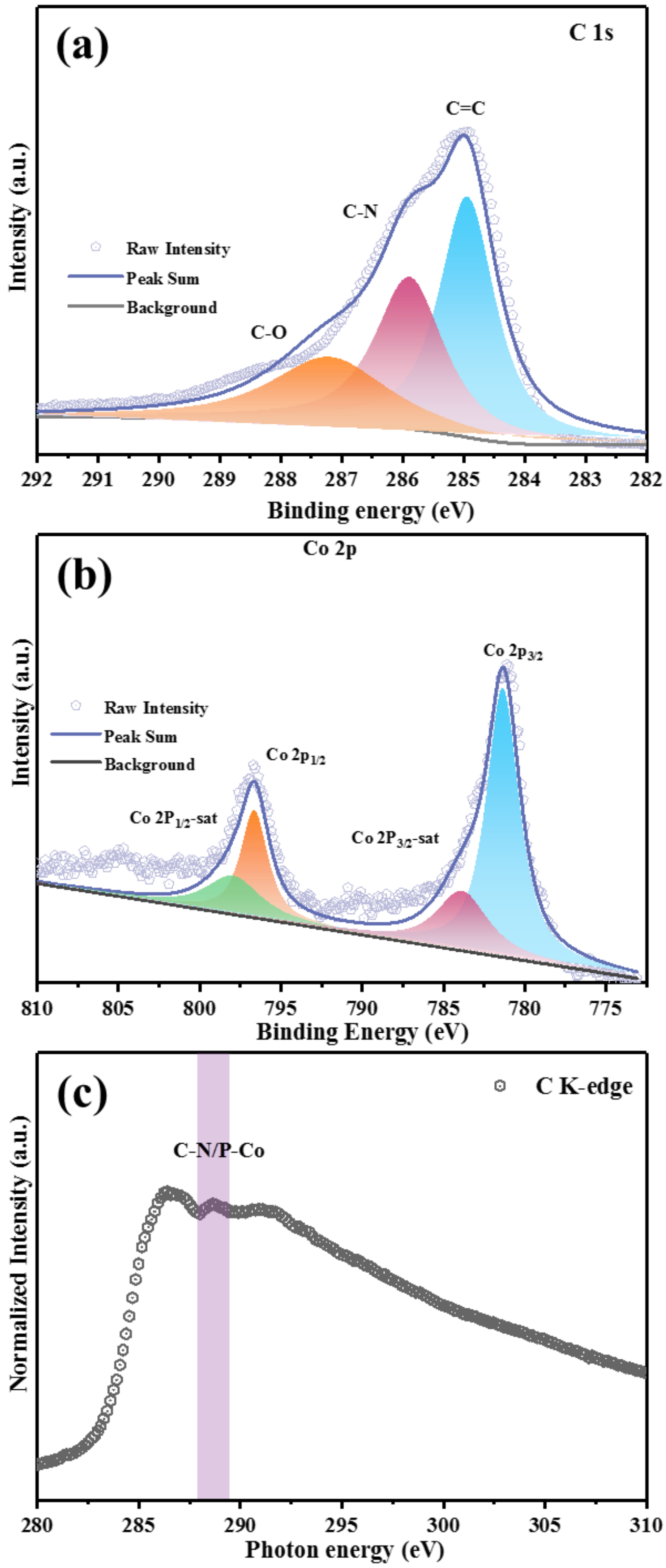

Supplementary Figure 4. Deconvoluted XPS spectrum of (a) C 1s and (b) Co 2p in Co-CNP, (c)the C K-edge XANES results of Co-CNP

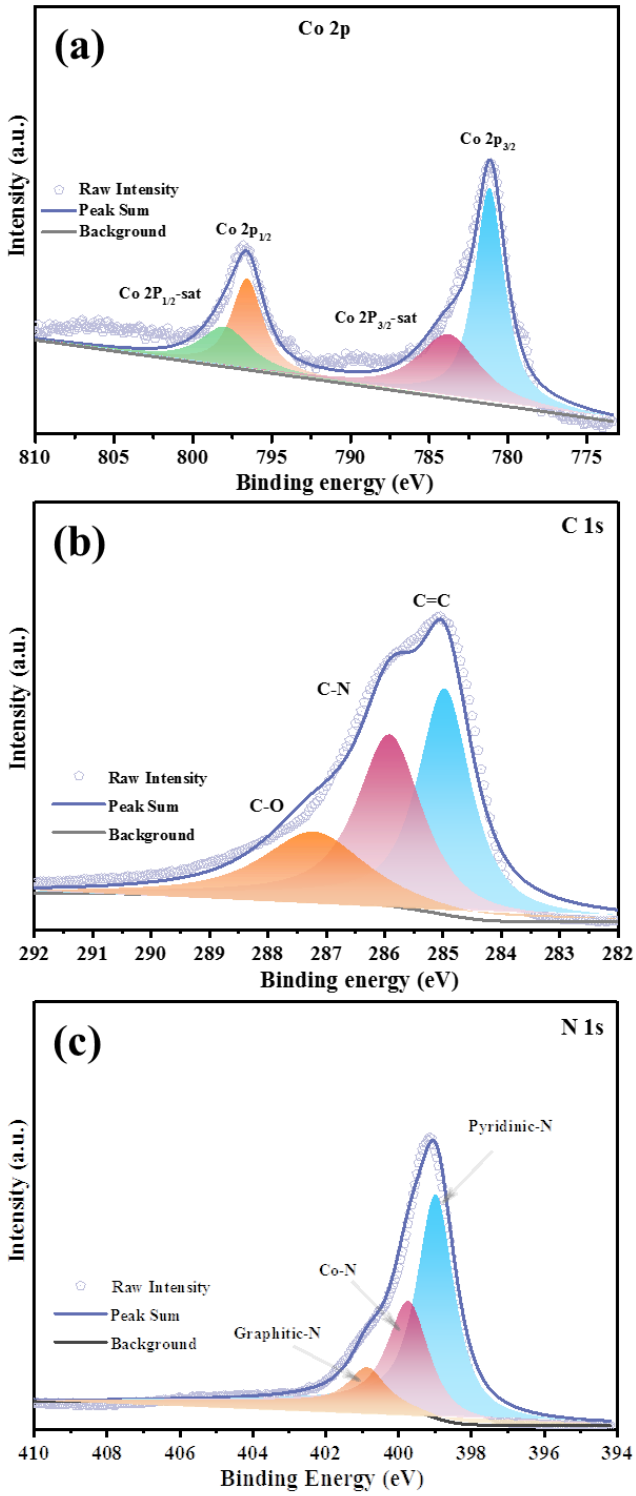

Supplementary Figure 5. Deconvoluted XPS spectra of (a) Co 2p, (b) C 1s, and (c) N 1s in Co-CN SAC with a high resolution.

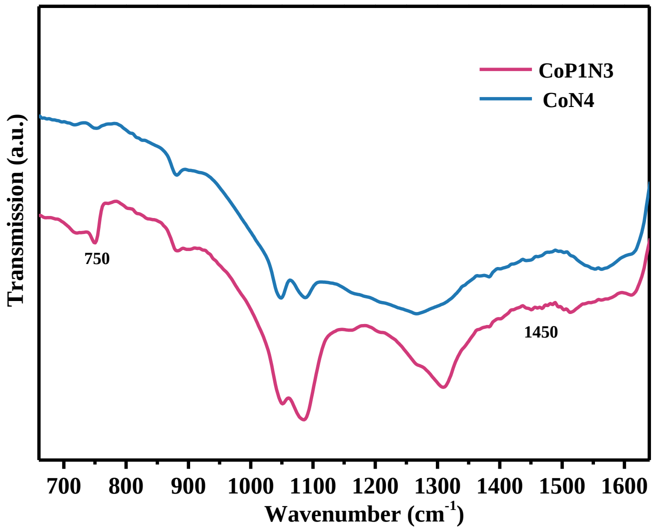

Supplementary Figure 6. FTIR spectra of the CoP1N3 and CoN4 samples.

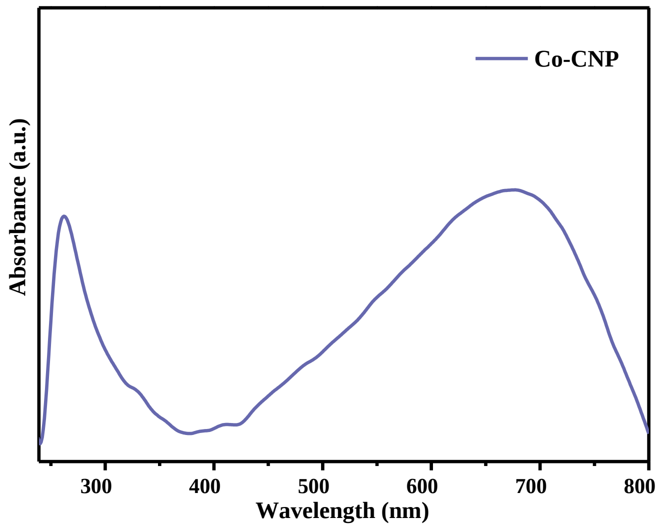

Supplementary Figure 7. UV–vis spectra of the Co-CNP samples.

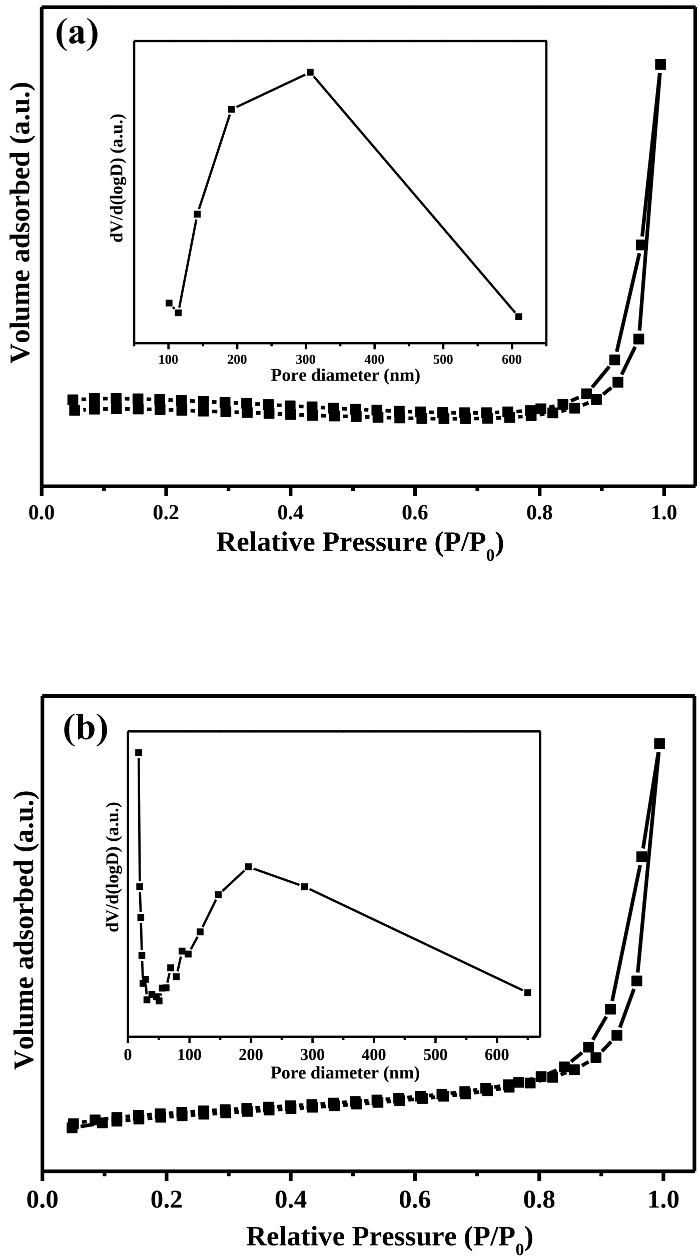

Supplementary Figure 8. N_2-sorption and the corresponding pore size distributions in the (a) Co-CN, (b) Co-CNP samples.

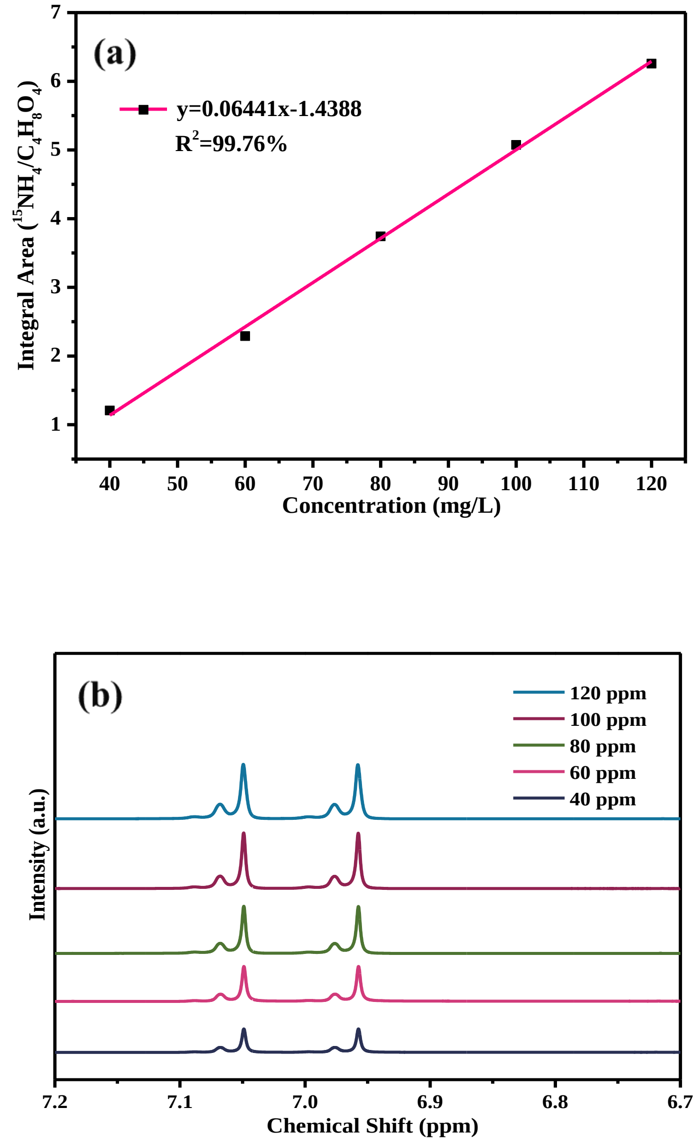

Supplementary Figure 9. (a) 1H NMR spectra (800 MHz) of standard $(^{15}NH_4)_2SO_4$ samples with different concentrations. (b) linear fitting of the integral area ratio ($^{15}N{-}^{15}NH_4^+/C_4H_4O_4$) and $^{15}N{-}^{15}NH_4^+$ concentration.

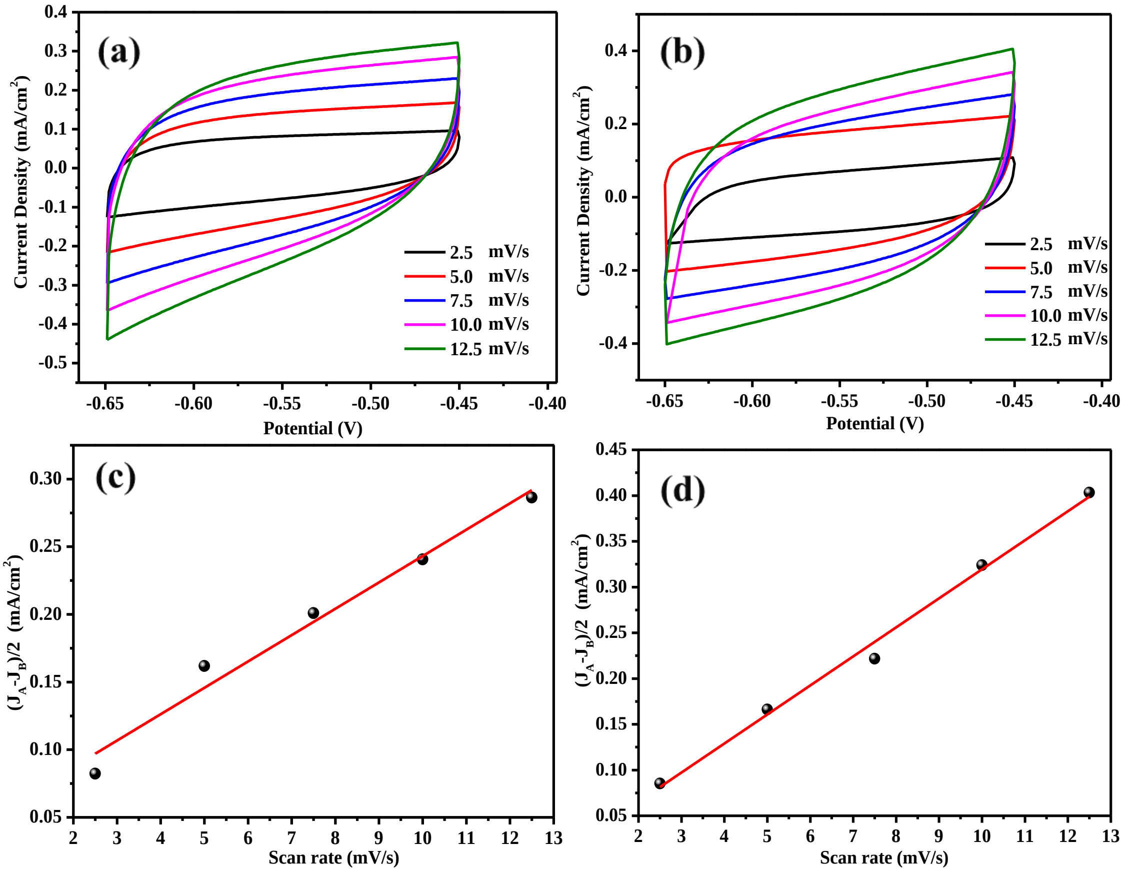

Supplementary Figure 10. The CV curves of Co-CN (a) and Co-CNP (b) at different scan rates in the non-Faradaic region; The capacitive current differences of $(J_A - J_B)/2$ as a function of rates in for Co-CN (c) and Co-CNP (d).

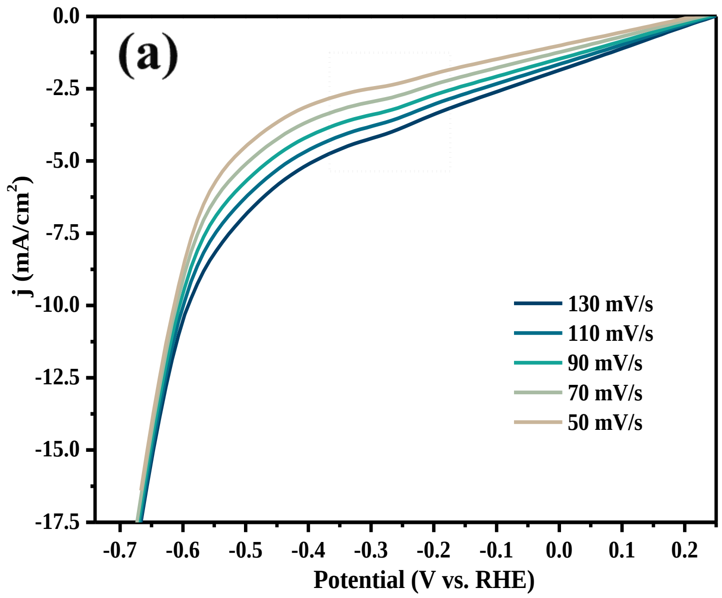

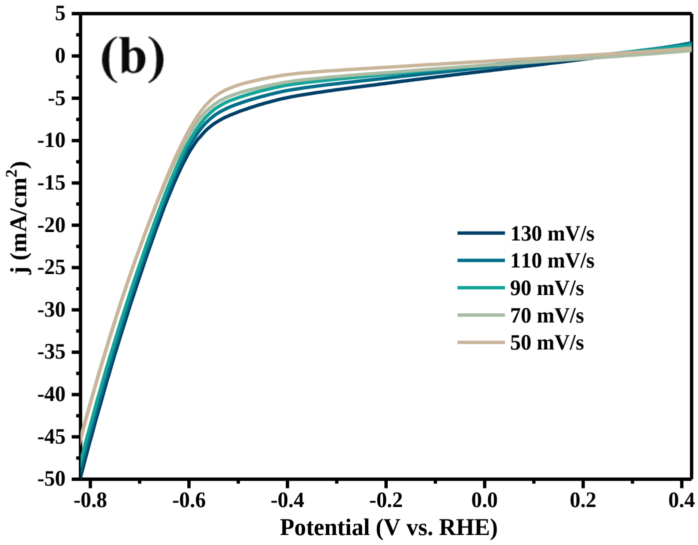

Supplementary Figure 11. (a) The LSV curves with different sweep rates for Co-CN at nitrates solution (a) and Co-CNP at nitrite solution (b).

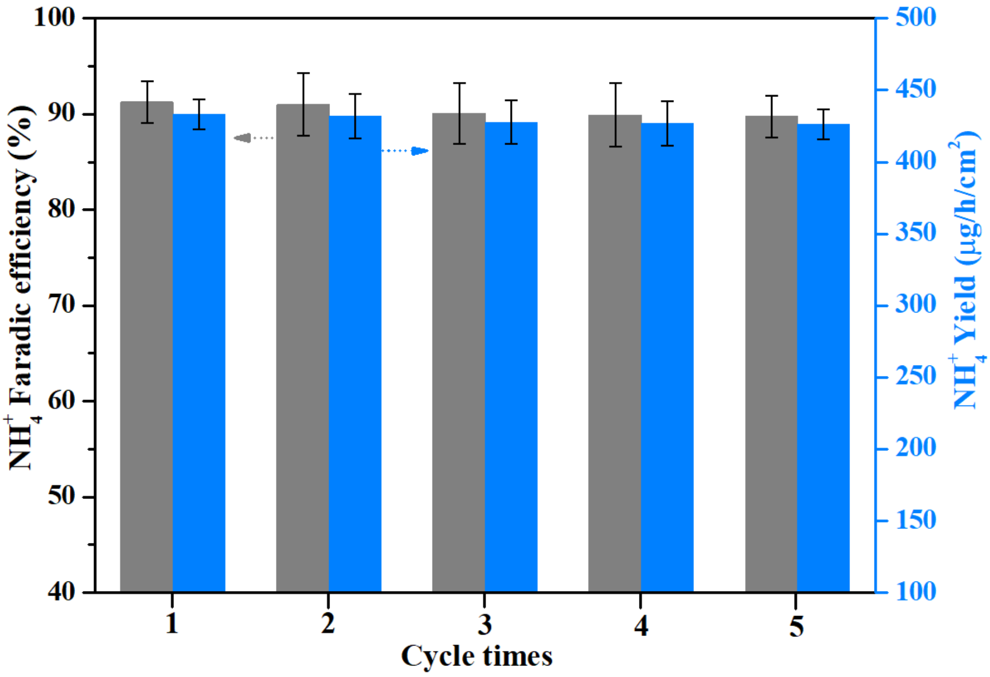

Supplementary Figure 12. Cycle Faradaic efficiency for NH_4^+ production and NH_4^+-yield on Co-CNP SACs.

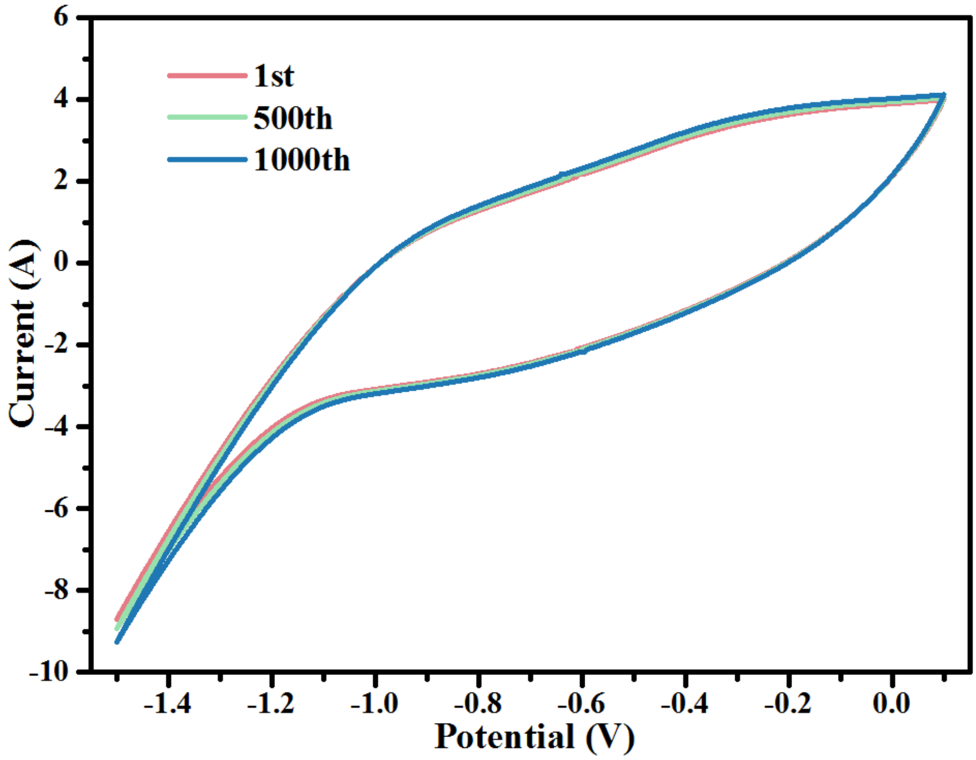

Supplementary Figure 13. CV results for Co-CNP with different cycle durations.

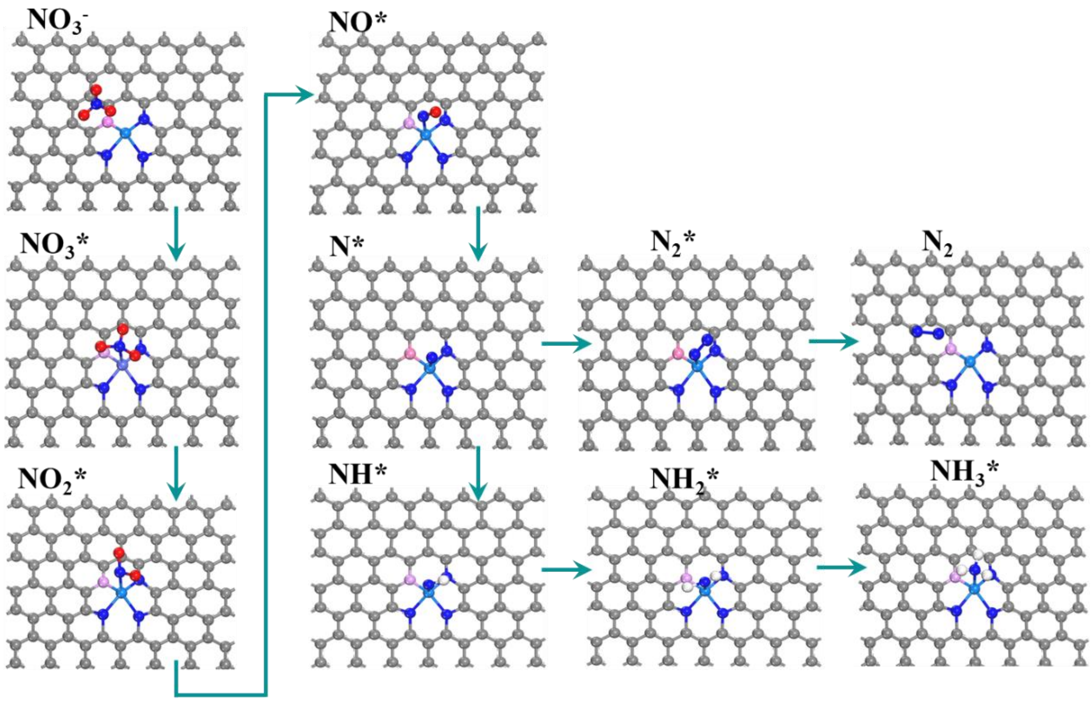

Supplementary Figure 14. The adsorption models on an ideal CoP_1N_3 site

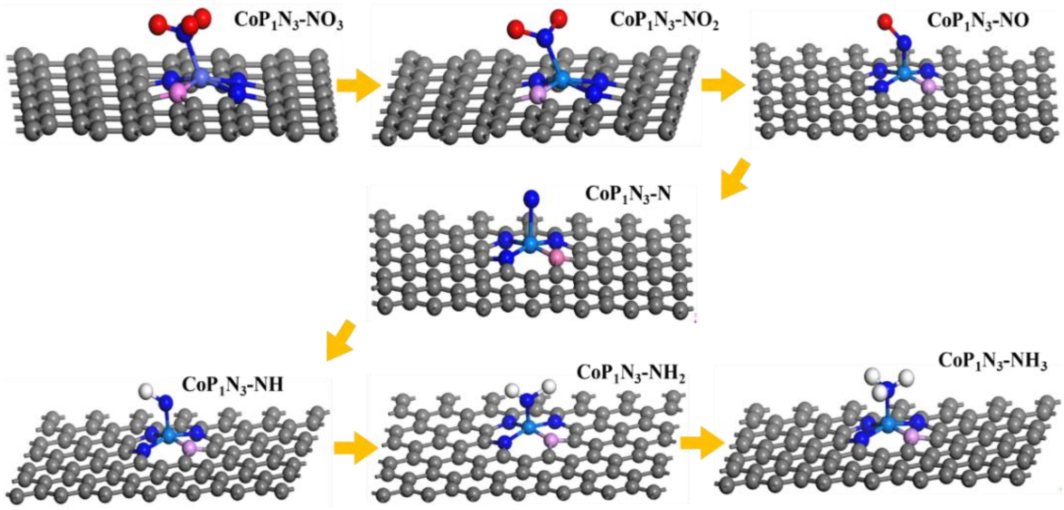

Supplementary Figure 15. The side-view of nitrate adsorption model on an ideal CoP_1N_3 site

Table S1. EXAFS fitting parameters for various samples.

Sample	Shell	*CN* [a]	*R*[Å] [b]	$\sigma^2(10^{-3})$ [c]	*R* factor [d]
Co-CN	Cu-N	4.1	1.92	6.3	0.009
Co-CNP	Co-N	3.2	1.94	5.1	0.018
	Co-P	0.9	2.21	5.1	

[a] *CN* is the coordination number, [b] *R* is the average bonding distance, [c] σ^2 is Debye–Waller factor and [d] *R* factor represents the fitting quality.

Table S2. Physical and chemical properties of samples.

Sample	S_{BET} (m^2/g)	V_{meso}[a] (cc/g)	d_{meso}[a] (nm)	ECSA (cm^2)
Co-CN	18.0	0.07	36.7	0.49
Co-CNP	35.4	0.12	24.2	0.79

[a] Mesopore volume and diameter were obtained from the N_2-desorption branch using the BJH method.

Table S3. Comparison of nitrate reduction in this study with previous reports.

No.	Cathode	Cathode Area (cm^2)	Anode	Solution conditions	NH_4^+-Faradaic efficiency (%)	NH_4^+-Yield rate	Ref.
1	Fe-PPy	0.25	-	0.1 M KOH + 0.1 M KNO_3	100	2.75 $mg_{NH3}\cdot h^{-1}\cdot cm^{-2}$	1
2	Cu/Cu_2O	1	platinum foil	0.5 M Na_2SO_4 200 ppm nitrate-N	95.8	-	2
3	Fe SAC	2	platinum foil	0.1 M K_2SO_4 and 0.5 M KNO_3	75	0.46 $mmol\cdot h^{-1}\cdot cm^{-2}$	3
4	TiO_{2-x} nanotube	1	platinum foil	0.5 M Na_2SO_4 +50 ppm NO_3^-−N	85	-	4
5	Cu-PTCDA	2	Platinum foil	PBS (0.1 M, pH=7) 500 ppm of NO_3^-	85.9	436 ± 85 $\mu g\cdot h^{-1}\cdot cm^{-2}$	5
6	Au/C	-	Pt wire	1 mM KNO_3 + 0.5 M K_2SO_4 (initial pH 3.5)	26	(4.4 ± 0.7) × 10^2 $pmol\cdot s^{-1}\cdot cm^{-2}$	6
7	Ti foil	0.3	glassy carbon plate	0.1 M HNO_3 + 0.3 M KNO_3	82	-	7
8	NiAlMnCoCu alloy	2	Pt plate	0.5 M KOH+0.05 M KNO_3	92.2	-	8
9	Co-CNP	2.25	Ti/IrO_2–Ru	0.02 M Na_2SO_4	92.0	433.3 $\mu g_{NH4}\cdot h^{-1}\cdot cm^{-2}$.	This Work

References

1. Li, P. P., Jin, Z. Y., Fang, Z. W., & Yu, G. H., A single-site iron catalyst with preoccupied active center that achieves selective ammonia electrosynthesis from nitrate. *Energy Environ. Sci.* **14**, 3522-3531 (2021).

2. Wang, Y., Zhou, W., Jia, R., Yu, Y. & Zhang, B., Unveiling the activity origin of a copper-based electrocatalyst for selective nitrate reduction to ammonia. *Angew. Chem. Int. Ed*. **59**, 5350-5354 (2020).

3. Wu, Z. Y. et al. Electrochemical ammonia synthesis via nitrate reduction on Fe single atom catalyst. *Nat. Commun.* **12**, 2870-2880 (2021).

4. Jia, R. R. et al. Boosting selective nitrate electroreduction to ammonium by constructing oxygen vacancies in TiO_2. *ACS Catal.* **10,** 3533-3540 (2020).

5. Chen, G.F. *et al.* Electrochemical reduction of nitrate to ammonia via direct eight-electron transfer using a copper–molecular solid catalyst. *Nat. Energy* **5,** 605–613 (2020).

6. Jaecheol, C. *et al.* Electroreduction of nitrates, nitrites, and gaseous nitrogen oxides: a potential source of ammonia in dinitrogen reduction studies. *ACS Energy Lett.* **5**, 2095−2097 (2020).

7. McEnaney, J. M. *et al.* Electrolyte engineering for efficient electrochemical nitrate reduction to ammonia on a titanium electrode. *ACS Sustainable Chem. Eng.* **8,** 2672–2681 (2020).

8. Lu, C., Lu, S. G., Qiu, W. H., Liu, Q. G. Electroreduction of nitrate to ammonia in alkaline solutions using hydrogen storage alloy cathodes. *Electrochimica Acta* **44**, 2193–2197 (1999).